

ARTICLE

Photoelectrochemical Alcohol Oxidation by Mixed-Linker Metal-Organic Frameworks

Shaoyang Lin, Daniel R. Cairnie, Dylan Davis, Arnab Chakraborty, Meng Cai, and Amanda J. Morris*

Received 00th January 20xx,
Accepted 00th January 20xx

DOI: 10.1039/x0xx00000x

Metal-organic frameworks (MOFs) provide a suitable platform for stable and efficient heterogeneous photoelectrochemical oxidation catalysis due to their highly ordered structure, large surface area, and synthetic tunability. Herein, a mixed-linker MOF comprising a photosensitizer $[\text{Ru}(\text{dcbpy})(\text{bpy})_2]^{2+}$ (bpy = 2,2'-bipyridine, dcbpy = 5,5'-dicarboxy-2,2'-bipyridine) and catalyst $[\text{Ru}(\text{tpy})(\text{dcbpy})\text{Cl}]^+$ (tpy = 2,2':6',2''-terpyridine) were incorporated into the UiO-67 framework and grown as thin films on a TiO_2 -coated, fluorine-doped tin oxide (FTO) electrode (RuB-RuTB-UiO-67- TiO_2 /FTO). When used as an electrode for the photoelectrochemical oxidation of benzyl alcohol, the mixed-linker MOF film showed a Faradaic efficiency of 34%, corresponding to a 3-fold increase in efficiency relative to a RuB-UiO-67- TiO_2 /FTO control. This increase in catalytic efficiency is ascribed to the activation of RuTB moieties via oxidation by photogenerated Ru^{III} . Transient absorption spectroscopy revealed the delayed appearance of $\text{Ru}^{\text{III}}\text{TB}^*$ or $\text{Ru}^{\text{III}}\text{TB}$ formation, occurring with a lifetime of 21 ns, due to energy and/or electron transfer. The recovery kinetics of the charge separated state was increased (283 μs) in comparison to single-component control experiments (105 μs for RuB-UiO-67- TiO_2 /FTO and 7 μs for RuTB-UiO-67- TiO_2 /FTO) indicating a cooperative effect that could be exploited in chromophore/catalyst MOF motifs.

Introduction

Metal-organic frameworks (MOFs) are a class of porous materials composed of metal ions or clusters joined together by organic linkers, forming hierarchical 1-, 2-, and 3-D structures. Given the inherent structural tunability that comes with their design, MOFs can exhibit high porosity, numerous morphologies, and structural stability in a wide variety of conditions, all from the modification of their constituent parts – linkers and nodes.¹ Additionally, when chromophores and/or catalysts are incorporated into the MOF structure, the framework adopts their photophysical, photochemical, and/or catalytic traits.^{2,3} Consequently, a large portion of the MOF literature focuses on their use as solid-state photocatalysts for H_2 evolution and CO_2 reduction.^{4–10} Early MOF photocatalysis was accomplished by dissolving a homogeneous photosensitizer in the reaction solution with dispersed catalytic MOF particles.^{4,5,10} In order to avoid the difficulty of photosensitizer reuse and separation, a few groups have been focusing on incorporating the light absorption species and catalysts into the MOF scaffold simultaneously.^{6–9} In 2018, Huang et al. reported the functionalization of UiO-67 with $[\text{Ru}(\text{dcbpy})(\text{bpy})_2]^{2+}$ (bpy = bipyridine, dcbpy = 5,5'-dicarboxy-2,2'-bipyridine) as the photosensitizer and $\text{Pt}(\text{dcbpy})\text{Cl}_2$ as the

catalyst for photochemical H_2 reduction.⁸ That same year, Lin and coworkers reported a hafnium-based 2D MOF, incorporating $[\text{Ru}(\text{dcbpy})(\text{bpy})_2]^{2+}$ and $\text{M}(\text{bpy})(\text{CO})_3\text{X}$ (M = Re or Mn, X = Cl, or Br) into the structure as a photocatalyst for CO_2 reduction.¹² In these prior examples, a sacrificial electron donor (SED) was used to provide the reducing equivalents needed for ultimate photoconversion. SEDs, while powerful for fundamental studies, can complicate reactivity. For example, catalytic intermediates formed between CO_2 reduction catalysts and triethanolamine (TEOA) have been found to promote highly unproductive back-electron transfer mechanisms.¹³

One way to circumvent the need for a sacrificial electron donors or acceptors is through the use of a semiconductor electrode that can act as an electron source or sink with or without an applied bias. This concept was first applied in 1999 as a dye-sensitized photoelectrosynthesis cell (DSPEC) that oxidized isopropanol to acetone with a Ru polypyridyl chromophore-catalyst assembly.¹⁴ The catalytic mechanism for this assembly first begins with excitation of a semi-conductor bound chromophore, followed by the excited-state injection into the semiconductor conduction band (CB), akin to the photovoltaic action of a dye-sensitized solar cell. The oxidized chromophore can then oxidize a co-bound or covalently attached catalyst, thus activating it to further reactivity. Since the advent of DSPECs, the application of chromophore-catalyst assemblies has been largely pioneered by Meyer et al. using Ru(II) polypyridyl motifs to perform water and alcohol oxidation.¹⁵ To our knowledge, there are only a small handful of instances where photoelectrochemical reactivity is studied in a MOF, mainly comprising mixed-metal and homoleptic MOF-

^a Address here.

^b Address here.

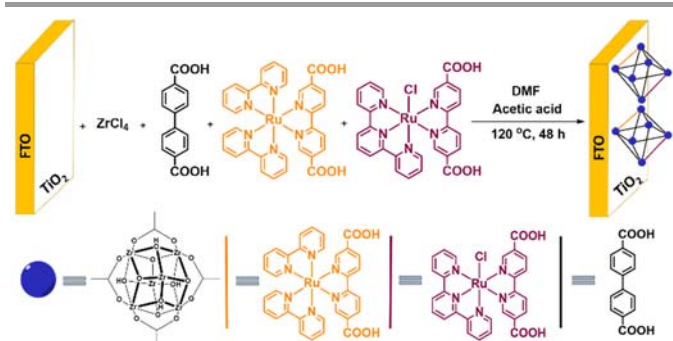
^c Address here.

† Footnotes relating to the title and/or authors should appear here.

Electronic Supplementary Information (ESI) available: [details of any supplementary information available should be included here]. See DOI: 10.1039/x0xx00000x

semiconductor composites, leaving the cooperative behaviour mechanisms between ligand active sites in MOFs still largely unexplored.^{14–16}

Our prior work with Ru(II) polypyridyl-based chromophores and catalysts incorporated into the Zr-based MOF, UiO-67, provides the foundation to explore Meyer-type chemistry in MOF constructs. We have previously demonstrated energy transfer between incorporated $[\text{Ru}(\text{dcbpy})(\text{bpy})_2]^{2+}$ (RuB) chromophores in UiO-67, as well as electron injection from these chromophores into TiO_2 nanoparticles.^{19–23} Our studies on water oxidation by $[\text{Ru}(\text{tpy})(\text{dcbpy})\text{H}_2\text{O}]^{2+}$ (RuTB, where tpy = 2, 2': 6', 2'-terpyridine) in UiO-67 have shown high aqueous stability, retention of the high catalytic activity of the parent catalyst, stabilization of the catalyst to deactivation pathways, and in-MOF reactivity.^{24–26} Herein, we report a mixed linker MOF grown on a nanoparticulate TiO_2 fluorine-doped tin oxide (FTO) electrode that incorporates RuB as the photosensitizer and RuTB as a catalyst for the photoelectrochemical oxidation of alcohol. The catalytic activity of RuTB-RuB-UiO-67/ TiO_2 /FTO was demonstrated by electrochemical and photoelectrochemical experiments. The mechanism of electron transfer between the photosensitizer RuB and catalyst RuTB inside the RuTB-RuB-UiO-67/ TiO_2 /FTO assembly was investigated via transient absorption spectroscopy. To our knowledge, this is the first example of photoelectrochemical oxidation chemistry by a MOF. The cooperative nature of the mixed MOF and semiconductor eliminated the need for sacrificial electron acceptors and provides a model for the future photoelectrochemical MOF cells.



Scheme 1. Direct solvothermal synthesis of the mixed-linker MOF film, RuB-RuTB-UiO-67/ TiO_2 /FTO, characterized in this work.

Experimental section

Materials:

All chemicals and solvents were used as obtained without further purification, including $\text{RuCl}_3 \cdot x\text{H}_2\text{O}$ (Acros, 35–40% Ru), 2,2'-bipyridyl-5,5'-dicarboxylic acid (dcbpy, Ark Pharm, Inc., 95%+), 2,2':6,2''-terpyridine (tpy, Alfa Aesar, 97%), 4,4'-biphenyldicarboxylic acid (bpdc, TCI, 97%), zirconium (IV) chloride (ZrCl_4 , Sigma–Aldrich, 98%), N,N-dimethylformamide (DMF, Fisher Scientific, HPLC grade, >99%), acetonitrile (Fisher Scientific, HPLC grade), acetic acid (Fisher Chemical, glacial), sodium hydroxide (NaOH, Spectrum, 97%), deuterium oxide

(D_2O , Cambridge Isotope Laboratories, Inc., 99.9%), benzyl alcohol (Sigma-Aldrich, >99.0%), benzaldehyde (Alfa-Aesar, >99%), sodium bicarbonate (NaHCO_3 , Acros, 99.5%), lithium perchlorate (LiClO_4 , Acros, >99%), isopropyl alcohol (Spectrum, HPLC grade), Alconox detergent (Alconox Inc.), acetone (Spectrum, HPLC grade) and titanium nanoxide (TiO_2 , T/SP, Solaronix). FTO slides were acquired from Hartford Glass, Inc.

Synthesis of RuB, $[\text{Ru}(\text{dcbpy})(\text{bpy})_2][\text{PF}_6]_2$:

The synthesis of RuB is followed by the modified method from literature.²⁰ Approximately 0.2 g $\text{Ru}(\text{bpy})_2\text{Cl}_2$, 0.15 g dcbpy and 0.2 g NaHCO_3 was refluxed in 40 ml MeOH/water (v/v, 4/1) mixture for 24 h under N_2 . The pH of the cooled solution was adjusted to ~ 4.4 by concentrated HNO_3 . Then the mixture was filtered and rotary evaporated to remove the precipitated dcbpy and residual MeOH. A KPF_6 solution (1 g in 10 ml water) was added dropwise until precipitation of RuB ceased. The product was then filtered and dried.

Synthesis of RuTB, $[\text{Ru}(\text{dcbpy})(\text{tpy})\text{Cl}]\text{Cl}$:

$[\text{Ru}(\text{dcbpy})(\text{tpy})\text{Cl}]\text{Cl}$ was synthesized according to the method described in our previous reports.²⁵

Preparation of RuB-UiO-67/FTO:

To prepare the FTO slide, it was cleaned by sequential sonication in Alconox/DI water, DI water, isopropanol and acetone, followed by drying in oven at 100 °C.

For film synthesis, approximately 0.25 mmol ZrCl_4 , 0.01 mmol RuB, 0.24 mmol biphenyl-4,4'-dicarboxylic acid (BPDC) and 0.5 ml acetic acid were dissolved in 10 ml DMF in a 6-dram vial. The mixture was sonicated for 20 min before placing a clean FTO slide into the vial conductive-side up. The vial was heated at 120 °C for 24 h in oven. After cooling to room temperature, the MOF film was washed with DMF and acetone then further soaked in acetone (fresh solvent replaced every 24 h for 3 d). Before experimentation, the films were air-dried for 24 h.

Preparation of RuTB-UiO-67/FTO:

The method of preparing RuB-RuTB-UiO-67/FTO is similar to RuB-UiO-67/FTO. Instead, 0.25 mmol ZrCl_4 , 0.01 mmol RuTB, 0.23 mmol bpdc and 0.5 ml acetic acid were mixed with 10 ml DMF in a 6-dram vial. From this point, the procedure follows the same format as the RuB-UiO-67/FTO synthesis.

Preparation of RuB-RuTB-UiO-67/FTO:

The method of preparing RuB-RuTB-UiO-67/FTO is similar to RuB-UiO-67/FTO. Instead 0.25 mmol ZrCl_4 , 0.01 mmol RuB, 0.01 mmol RuTB, 0.23 mmol BPDC and 0.5 ml acetic acid was mixed with 10 ml DMF.

Fabrication of TiO_2 /FTO:

Titanium nanoxide (T/SP, Solaronix) was deposited on the conducting side of FTO by doctor blade method. The slide was heated at 100 °C for 2 h before heated at 450 °C for 30 min and cooled to room temperature.

Preparation of RuB-UiO-67/ TiO_2 /FTO, RuTB-UiO-67/ TiO_2 /FTO and RuB-RuTB-UiO-67/ TiO_2 /FTO films:

RuB-UiO-67/TiO₂/FTO and RuB-RuTB-UiO-67/TiO₂/FTO were fabricated using the similar method discussed above in the presence of a TiO₂/FTO substrate.

Powder X-ray diffraction (PXRD):

A 600 W Rigaku MiniFlex powder diffractometer with a CuK α ($\lambda = 1.5418 \text{ \AA}$) radiation source was used, with a sweeping range of 2–25° in continuous scanning mode. PXRD traces were collected in 0.05° increments at a scanning rate of 0.2°/min.

Scanning electron microscopy (SEM):

A LEO (Zeiss) 1550 field-emission scanning electron microscope, equipped with an in-lens detector, operating at 5.0 kV was used to obtain high-resolution images of the MOF particles.

Inductively-coupled plasma-mass spectrometry (ICP-MS):

The MOF thin films of RuB-RuTB-UiO-67/TiO₂/FTO were digested in 70 % nitric acid at 80 °C for 6 h. The solution was then diluted 10 times. Thermo Electron X-Series inductively coupled plasma mass spectrometer in accordance with Standard Method 3125-B was applied to determine the ruthenium and zirconium contents in the samples.

Photoelectrochemical alcohol oxidation:

Photoelectrolysis experiments were conducted in a two-compartment cell separated by a frit. Photocurrent response was recorded by a BASi Epsilon potentiostat instrument. RuB-RuTB-UiO-67/TiO₂/FTO was served as working electrode, with Pt mesh as counter electrode and Ag/Ag⁺ (0.01 M, AgNO₃) as reference electrode. The Ag/Ag⁺ electrode was calibrated against the ferrocene redox couple (Fc/Fc⁺, 0.4 V vs NHE in MeCN). The electrolyte was prepared by dissolving 1.06 g LiClO₄ in 100 ml BnOH/MeCN (5/95, v/v) solvent. Each photoelectrochemical oxidation experiment test went for 2 h with a bias potential (0.6 V vs NHE) after purging the cell with N₂ for 30 min. The light shined at the working electrode was from a Xe lamp with a 455 nm cut-on filter.

Product analysis:

The amount of product, benzaldehyde (BZH) was quantified by an Agilent 7890C with an FID detector. After the photocatalysis experiments, 1 μ L of the electrolyte solvent was used for gas chromatography. The concentration of BZH in the sample was determined by the calibration curve obtained from the measurement of standard samples.

MOF NMR digestion:

A 1M NaOD/D₂O mixture (1 mL) was used to dissolve 5.0 mg of the residual MOF powder made during film synthesis. The mixture was sonicated for 10 min and filtered through a pipette packed with glass wool to remove any precipitated salts. NMR data was then collected from the filtrate.

Steady-state absorption spectroscopy:

Steady-state absorption spectrum of the ligand or thin films in solution and diffuse reflectance spectra of MOF powder were collected using a Cary 5000 UV-vis NIR spectrometer.

Steady-state and time-resolved emission spectroscopy:

Steady-state and time-resolved emission measurements were performed with a 532 nm Nd:YAG laser (Spectra-Physics-Quanta-Ray Lab) operating at 1 Hz. To collect the steady-state measurements, an LP980 laser flash photolysis system (Edinburgh Instruments), with an image-intensified CCD camera detector (Andor i-Star ICCD) was used. The time-resolved measurements were recorded with an R928 PMT detector (Hamamatsu).

Nanosecond transient absorption spectroscopy:

Transient absorption spectroscopic measurements were conducted with an LP980 laser flash photolysis system (Edinburgh Instruments) and 532 nm Nd:YAG laser (Spectra-Physics-Quanta-Ray Lab) operating at 1 Hz and 7–8 mJ per pulse. The kinetic measurements were collected with an R928 PMT detector (Hamamatsu). The steady-state measurements and time-delayed spectral mapping were collected with an ICCD camera (Andor i-Star) gated to 10 ns.

Results and discussion

RuB-RuTB-UiO-67-TiO₂/FTO MOF thin films along with the RuB and RuTB ligands were synthesized from previously established procedures by our group (Scheme 1, *vide supra*).^{23,25} When RuB and RuTB were added to a solvothermal mixture in a 1:1 molar ratio, the resulting MOF film comprised the two incorporated chromophores as a 1.5:1 ratio of RuB to RuTB (confirmed via ¹H-NMR, Supporting Information, Figure S3). The powder X-ray diffraction (PXRD) data of RuTB-RuB-UiO-67 aligned with the simulated pattern of UiO-67 quite well, indicating that the crystal structure was maintained after linker doping with RuB and RuTB (Figure 1A). The typical UiO-67 octahedral particle shape was observed in SEM images of RuTB-RuB-UiO-67 (Figure 1B). The thickness of nanoparticulate TiO₂ films was found to be 6 μ m. When the MOF film was deposited on the nanoparticles, the MOF penetrated throughout the nanoparticulate TiO₂ network as well as extended beyond the surface of the TiO₂ by 3 μ m. The diffuse reflectance UV-Vis spectrum of the residual RuTB-RuB-UiO-67 powder from the TiO₂/FTO film synthesis was recorded. The characteristic ¹MLCT absorption bands for RuB and RuTB were observed in the composite spectrum (Figure 1C).

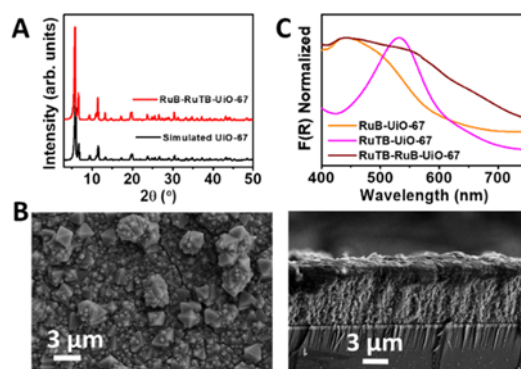


Figure 1. A) PXRD pattern of RuB-RuTB-UiO-67 matches with undoped UiO-67; B) Top view and side view of SEM images of RuTB-RuB-UiO-67/TiO₂/FTO; C) DR-UV-Vis spectrum of RuB-UiO-67 (orange), RuTB-UiO-67 (magenta) and RuTB-RuB-UiO-67 (maroon), confirming the incorporation of both RuTB and RuB inside the framework.

The photoelectrochemical properties and the catalytic activity towards photo-induced alcohol oxidation of RuTB-RuB-UiO-67/TiO₂/FTO were investigated. The cyclic voltammograms of RuTB-RuB-UiO-67/TiO₂/FTO in a 0.1 M LiClO₄ solution in MeCN displayed two reversible peaks with $E_{1/2}$ at 0.92 V vs NHE and 1.38 V vs NHE assigned to the redox couples, Ru^{II}TB/Ru^{III}TB and Ru^{II}B/Ru^{III}B, respectively (Figure 2A). Thus, thermodynamically Ru^{III}B can promote the oxidation of Ru^{II}TB, consistent with the literature.^{27,28} The current responses in the dark and light were recorded during linear sweep voltammetry in a 0.1 M LiClO₄, BnOH/MeCN (v/v, 5/95) mixture (Figure 2B). Under white light illumination (> 455 nm), an increase in the catalytic current was observed throughout the scanned potential window. Quantified at a constant bias potential (0.87 V vs NHE), RuB-RuTB-UiO-67/TiO₂/FTO exhibited almost a two-fold increase in current (-32.2 μ A vs 17.2 μ A) upon light exposure.

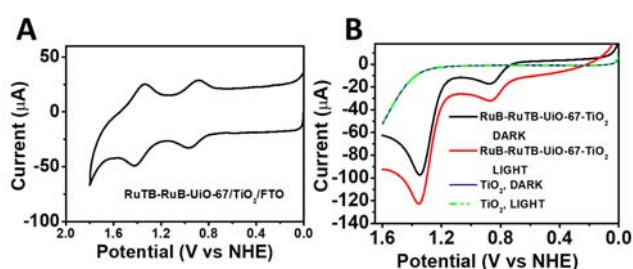


Figure 2. A) Redox current wave of RuTB(II/III) and RuB(II/III) observed from CV in 0.1 M LiClO₄, MeCN; B) LSV of RuTB-RuB-UiO-67/TiO₂/FTO in 0.1 M LiClO₄, BnOH/MeCN (v/v, 5/95) under dark or the light of 350 W Xe lamp with 455 nm cut-on filter.

To further investigate the photocurrent response of RuB-RuTB-UiO-67-TiO₂/FTO, a chopped-light experiment was conducted in the presence and absence of BnOH at a constant bias potential (0.6 V vs NHE) (Figure 3A). Interestingly, in the absence of BnOH, both RuB-RuTB-UiO-67-TiO₂/FTO and a RuB-UiO-67-TiO₂/FTO control exhibit similar photocurrent. This perhaps would not be expected given one might assume RuB to be a superior photosensitizer to RuTB. In both samples, care was taken to keep the amount of incorporated Ru consistent. Therefore, when RuTB was incorporated into the framework at a ratio of 1:1.5 (RuTB:RuB) (Supporting Information, Figure S3), the amount of RuB decreases in comparison to the RuB-UiO-67-TiO₂/FTO control. It was previously demonstrated by Meyer et al. that RuTB can attain comparable electron injection efficiencies to that of RuB anchored on TiO₂, making it a suitable photosensitizer.²⁸ Our results confirm that under the white light illumination conditions used for the chopped light experiment that the electron injection efficiency of RuB and RuTB are approximately equal and the amount of photocurrent is maintained.

After the introduction of BnOH, both RuB-RuTB-UiO-67-TiO₂/FTO and RuB-UiO-67-TiO₂/FTO display an increase in the observed photocurrent indicative of BnOH oxidation. The increase in current observed for RuB-UiO-67-TiO₂/FTO indicates RuB is a competent catalyst for BnOH oxidation. However, the rate of catalysis by RuB is slower than the diffusion of substrate

to the RuB centers as evidenced by the sharp drop in photocurrent upon light introduction. When RuTB was present, the current increased by a factor of two over that of the RuB control (-30.5 μ A vs -14.7 μ A, respectively). Additionally, the photocurrent exhibited a plateau, indicating a non-diffusion limited process and the superior catalytic rate of RuTB compared to RuB.

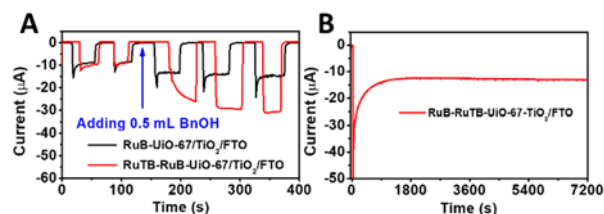


Figure 3. A) Photocurrent of RuB-UiO-67/TiO₂/FTO (black) and RuTB-RuB-UiO-67/TiO₂/FTO (red) before and after adding BnOH; B) Photoelectrocatalytic current profile of RuTB-RuB-UiO-67/TiO₂/FTO during the 2 h reaction.

Bulk photo-electrolysis was conducted in a two-compartment electrochemical cell to quantify the yield of benzaldehyde (BZH). The mixed-linker MOF film produced 190 \pm 30 nmol of BZH compared to 63 \pm 15 nmol for the RuB-UiO-67-TiO₂/FTO film and negligible product for TiO₂/FTO alone. TiO₂ was not expected to be active under the experimental conditions considering the applied potential and filtered light were not capable of promoting hole formation in the TiO₂ valence band. Consistent with the chopped-light experiment, the photocurrent for the bulk photoelectrolysis was the largest for the RuB-RuTB-UiO-67-TiO₂/FTO film at a steady-state value of 13 μ A (Figure 3B). The amount of BZH was quantified via gas chromatography with toluene as the internal standard (Supporting Information, Figure S4). The Faradaic efficiency of the two films, RuB- and RuB-RuTB-TiO₂/FTO, were 11 and 34%, respectively.

Table 1. Product analysis and yield of benzaldehyde.

	Charge Passed (C)	Yield (nmol)	Faradaic Efficiency (%)
TiO ₂	0.04 \pm 0.01	-	-
RuB-UiO-67/TiO ₂ /FTO	0.11 \pm 0.03	63 \pm 15	11 \pm 1
RuB-RuTB-UiO-67/TiO ₂ /FTO	0.11 \pm 0.02	190 \pm 30	34 \pm 10

To gain insight in the electron transfer process during the catalysis, the energetics of RuB-RuTB-UiO-67/TiO₂/FTO were investigated. The redox potential of Ru^{III}B/Ru^{II}B* was determined with the following relation:

$$E_{1/2}(\text{Ru}^{\text{III}}/\text{Ru}^{\text{II}}) = E_{1/2}(\text{Ru}^{\text{III}}/\text{Ru}^{\text{II}}) - \Delta G_{es} \quad (1)$$

where $E_{1/2}(\text{Ru}^{\text{III}}/\text{Ru}^{\text{II}})$ is the ground state redox couple Ru^{III}B/Ru^{II}B and ΔG_{es} is the free energy in the excited state.²⁹ ΔG_{es} was obtained from the intersection of a tangent line fit along the high energy side of the emission spectrum of RuB (Figure 4A). The value calculated was -0.88 V vs NHE, which is consistent with literature values.^{30,31} To determine the energetic position of the conduction band density of states (DOS) in TiO₂, the absorption of electrons in the conduction band of TiO₂ was monitored at 800 nm as a function of applied bias. Consistent

with the literature,³² the DOS appear as an exponential tail beginning at ~ -0.4 V vs NHE (Figure 4B). Approximately 1.4 mC/cm^2 of available electronic states are present at the redox potential of $\text{Ru}^{\text{III}}\text{B}/\text{Ru}^{\text{II}}\text{B}^*$, allowing electron injection from $\text{Ru}^{\text{II}}\text{B}^*$ to the TiO_2 conduction band, $\text{TiO}_2(\text{CB})$. Compiling the energetic data into a scheme clearly shows a potential path for a cooperative photoelectrocatalytic mechanism (Figure 5).

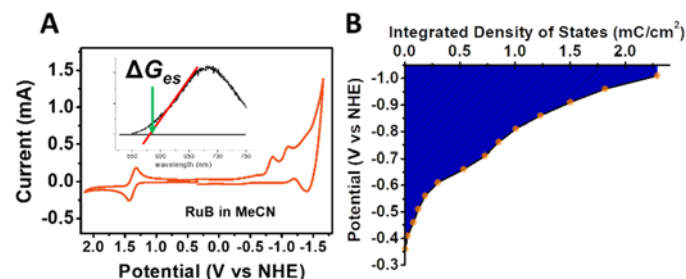


Figure 4. A) Cyclic voltammogram of the $\text{Ru}^{\text{II}}\text{B}/\text{Ru}^{\text{III}}\text{B}$ redox couple in MeCN, along with the determination of the excited-state free energy in $\text{Ru}^{\text{II}}\text{B}^*$ (inset), and B) the density of states (DOS) of TiO_2 in 0.1 M LiClO_4 ($5:95$ v/v) BnOH/MeCN .

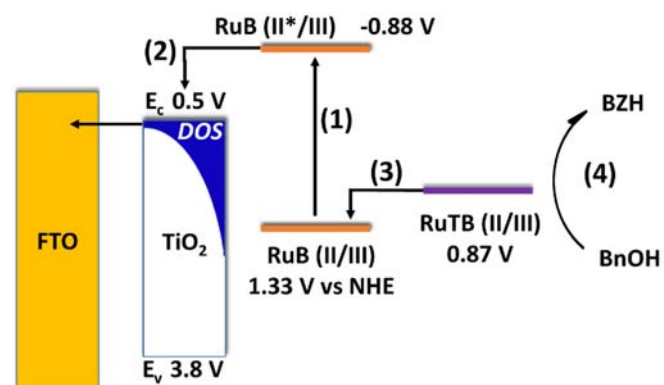


Figure 5. Energy diagram detailing the mechanism of photoelectrocatalysis in $\text{RuB-RuTB-UiO-67-TiO}_2/\text{FTO}$: (1) photoexcitation of $\text{Ru}^{\text{II}}\text{B}$ to $\text{Ru}^{\text{II}}\text{B}^*$; (2) electron injection from the LUMO of $\text{Ru}^{\text{II}}\text{B}^*$ into the CB of TiO_2 , thereby generating a hole that forms $\text{Ru}^{\text{III}}\text{B}$; (3) oxidation of $\text{Ru}^{\text{II}}\text{TB}$ by $\text{Ru}^{\text{III}}\text{B}$ to form $\text{Ru}^{\text{III}}\text{TB}$; and (4) oxidation of BnOH by $\text{Ru}^{\text{III}}\text{TB}$ to form BZH .

To determine if the proposed mechanism is operative, nanosecond transient absorption (TA) was conducted. The steady state TA spectrum (probed ~ 10 ns after the laser excitation) of $\text{RuB-UiO-67}/\text{FTO}$ matches with the spectrum of dissolved RuB in MeCN (Supporting Information, Figures S5 and S6). In both spectra, excited state absorption and ground state bleach can be found at 390 nm and 450 nm, respectively, indicating that the photophysical behaviour of RuB excitation state is retained upon MOF incorporation.^{8,9,32,33} However, when the MOF was grown on TiO_2 , the excited state absorption of $\text{RuB-UiO-67}/\text{TiO}_2/\text{FTO}$ significantly diminished due to electron injection into the $\text{TiO}_2(\text{CB})$ and the formation of $\text{Ru}^{\text{III}}\text{B}$ (Supporting Information, Figure S7). It is important to note that the degree of $\text{Ru}^{\text{II}}\text{B}^*$ excited state quenching by the $\text{TiO}_2(\text{CB})$ varied from sample to sample due to the different distribution of Ru sites within the MOF from batch to batch. Energy transfer and subsequent injection from RuB-UiO-67 into TiO_2/FTO electrodes was previously determined to occur up to 25 nm

from the TiO_2 surface.²³ Therefore, RuB centers further from the TiO_2 than 25 nm should simply decay via radiative and non-radiative pathways. Electron injection from $\text{Ru}^{\text{II}}\text{B}^*$ into $\text{TiO}_2(\text{CB})$ generally occurs on sub-nanosecond time scales, thus this process will not be discussed further.

The transient absorption spectra of RuB- , RuTB- , and $\text{RuB-RuTB-UiO-67-TiO}_2/\text{FTO}$ with respect to time were mapped and the kinetic of the ground-state bleach recovery measured at 500 nm (Supporting Information, Figures S10-S12). The TA spectra for RuB and RuTB show characteristics consistent with both dye injection into TiO_2 and excited-state decay. The decay of the transients would then involve both electron recombination ($\text{TiO}_2(e^-)$ to oxidized chromophore) and excited state decay (radiative and non-radiative). The complicated nature of these overlapping properties as well as the heterogeneous nature of TiO_2 film functionalization (distance between chromophores and the surface, distribution of surface states in TiO_2 , etc.) does not lend itself to discrete fitting by exponential decays. Therefore, the lifetimes for the ground state recovery were fit to a Kohlrausch-Williams-Watt (KWW) kinetic model, previously used to describe decay kinetics in DSSC constructs.^{28,34,35} The average lifetime, τ_{avg} , for RuB and RuTB were 105 ± 1 μs and 7.16 ± 0.08 μs , respectively. The shorter lifetime for RuTB in comparison to RuB is consistent with both the shorter excited state lifetime of RuTB and $\text{TiO}_2(e^-)$ recombination in the Marcus inverted region.

The TA spectra for $\text{RuB-RuTB-UiO-67-TiO}_2/\text{FTO}$ showed consistent characteristics with the controls, however, with one critical difference (Figure 6A). The ground state bleach from RuB (major component) and RuTB (minor component) as well as the corresponding quenched excited state absorptions are observed. However, the isosbestic point ($\Delta\text{O.D.} = 0$) exhibits a bathochromic shift from 555 to 620 nm as a function of time (Figure 6B). The isosbestic point from the $\text{RuB-UiO-67-TiO}_2/\text{FTO}$ control was observed at 555 nm and the isosbestic point for the $\text{RuTB-UiO-67-TiO}_2/\text{FTO}$ control occurred at 620 nm. As injection into the $\text{TiO}_2(\text{CB})$ occurs on a timescale faster than the resolution of the nanosecond measurement, the isosbestic shift is not consistent with electron injection into the $\text{TiO}_2(\text{CB})$ and rather is indicative of delayed formation of $\text{Ru}^{\text{III}}\text{TB}^*$ or $\text{Ru}^{\text{III}}\text{TB}$. Formation of the $\text{Ru}^{\text{III}}\text{TB}^*$ could occur via energy transfer between the $\text{Ru}^{\text{II}}\text{B}^*$ and RuTB , as has previously been observed.²⁸ $\text{Ru}^{\text{III}}\text{TB}$ could be formed via oxidation by the $\text{Ru}^{\text{III}}\text{B}$ formed upon photoexcitation and subsequent electron injection in the $\text{TiO}_2(\text{CB})$. The lifetime for the isosbestic point shift, τ_{isos} , was determined by the delayed growth at 550 nm as 21.0 ± 0.3 ns (Figure 6C).

The recovery kinetics at the bleach for $\text{RuB-RuTB-UiO-67-TiO}_2/\text{FTO}$ are complicated by the overlaying species and the decay processes of those species (enumerated below).

- 1.) $\text{Ru}^{\text{III}}\text{TB} + \text{TiO}_2(e^-) \rightarrow \text{Ru}^{\text{II}}\text{TB}$ (electron recombination)
- 2.) $\text{Ru}^{\text{III}}\text{B} + \text{TiO}_2(e^-) \rightarrow \text{Ru}^{\text{II}}\text{B}$ (electron recombination)
- 3.) $\text{Ru}^{\text{II}}\text{B}^* \rightarrow \text{Ru}^{\text{II}}\text{B}$ (excited state decay)

- 4.) $\text{Ru}^{\text{II}}\text{TB}^* \rightarrow \text{Ru}^{\text{II}}\text{TB}$ (excited state decay)
- 5.) $\text{Ru}^{\text{III}}\text{B} + \text{Ru}^{\text{II}}\text{TB} \rightarrow \text{Ru}^{\text{II}}\text{B} + \text{Ru}^{\text{III}}\text{TB}$ (electron transfer)
- 6.) $\text{Ru}^{\text{II}}\text{B}^* + \text{Ru}^{\text{II}}\text{TB} \rightarrow \text{Ru}^{\text{II}}\text{B} + \text{Ru}^{\text{III}}\text{TB}$ (energy transfer)

At long time scales (> 150 ns), electron transfer, energy transfer, and excited state decay processes are complete and contribute minimally to the recovery kinetics.^{27,28} Therefore, the recovery kinetics should be dominated by electron recombination to oxidized species (dominated by $\text{Ru}^{\text{III}}\text{TB}$, as evidenced by the transient absorption spectrum). The recovery kinetics were satisfactorily fit to two stretched exponential functions at 500 nm with τ_{avg} s of $5.8 \pm 0.3 \mu\text{s}$ and $283 \pm 2 \mu\text{s}$. The increase in the average lifetime of the decay kinetics observed in the mixed-linker MOF compared to the controls, RuB-UiO-67-TiO₂/FTO (105 μs) and RuTB-UiO-67-TiO₂/FTO (7 μs), establishes a cooperative effect in the mixed-MOF approach to extending the lifetime of charge separated states. We propose that the cooperative effect emerges due to a distance dependence to recombination, i.e. $\text{Ru}^{\text{III}}\text{TB}$ generated further away from the TiO₂ surface would result in slower through-space recombination.²⁶ We further would propose that the electron transfer pathway for generating $\text{Ru}^{\text{III}}\text{B}$, as opposed to energy transfer to $\text{Ru}^{\text{II}}\text{TB}$ and subsequent injection by the $\text{Ru}^{\text{II}}\text{TB}^*$, would be the dominant source of these long-lived states, although additional studies are needed to provide further support.

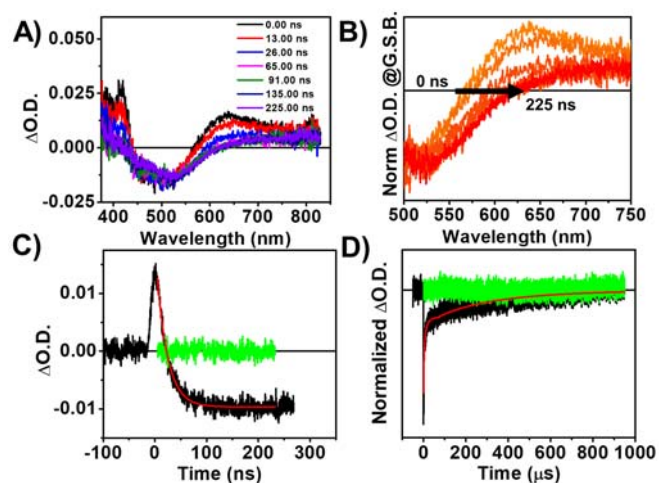


Figure 6. A) Transient absorption mapping of RuB-RuTB-UiO-67-TiO₂/FTO from initial excitation to 225 ns. B) Normalized TAS mapping at the ground-state bleach, showing the shift in isosbestic point with respect to time. C) The kinetic trace of RuB-RuTB-UiO-67-TiO₂/FTO probed at the isosbestic point, with an ascribed lifetime of 21 ± 0.3 ns. D) The kinetic trace for the ground state bleach at 500 nm fit to a Kohlrausch-Williams-Watt decay function, with an average lifetime of $283 \pm 2 \mu\text{s}$.

Conclusions

A mixed-linker MOF film was grown on a TiO₂/FTO substrate, incorporating the photosensitizer $[\text{Ru}(\text{dcbpy})(\text{bpy})_2]^{2+}$ and catalyst $[\text{Ru}(\text{tpy})(\text{dcbpy})\text{OH}_2]^{2+}$ into the framework structure, denoted as RuTB-RuB-UiO-67/TiO₂/FTO. The film was then used in the photoelectrochemical oxidation of benzyl alcohol and displayed Faradaic efficiency of 34%. This efficiency was a three-fold increase compared to that observed in the control films,

owing itself to the enhanced oxidation of $\text{Ru}^{\text{II}}\text{TB}$ centers by $\text{Ru}^{\text{III}}\text{B}$, therefore promoting catalysis with $\text{Ru}^{\text{III}}\text{TB}$. Given that the $\text{Ru}^{\text{III}}\text{B}$ redox potential is higher than that of $\text{Ru}^{\text{III}}\text{TB}$, electron transfer from the catalyst to the oxidized photosensitizer is a thermodynamically-favorable mechanism to enhance photocatalysis. Transient absorption spectroscopy revealed an isosbestic point shift attributed to the delayed growth of $\text{Ru}^{\text{III}}\text{TB}/\text{Ru}^{\text{II}}\text{TB}$ via oxidation by $\text{Ru}^{\text{II}}\text{B}$ or energy transfer from $\text{Ru}^{\text{II}}\text{B}^*$. The lifetime of the delayed process, τ_{isos} , was 21 ns. Fitting the ground-state bleach kinetics of RuTB-RuB-UiO-67/TiO₂/FTO to a stretched exponential model show a long-lived charge separated state with a τ_{avg} of 283 μs , a near 3-fold increase in charge-separated lifetime compared to the single-component controls RuB-UiO-67-TiO₂/FTO (105 μs) and RuTB-UiO-67-TiO₂/FTO (7 μs). With the successful incorporation of a known photosensitizer-catalyst system into a MOF architecture, this study highlights their potential to exhibit beneficial cooperative effects and serve as suitable candidates for oxidative photoelectrochemical catalysis.

Conflicts of interest

There are no conflicts to declare.

Acknowledgements

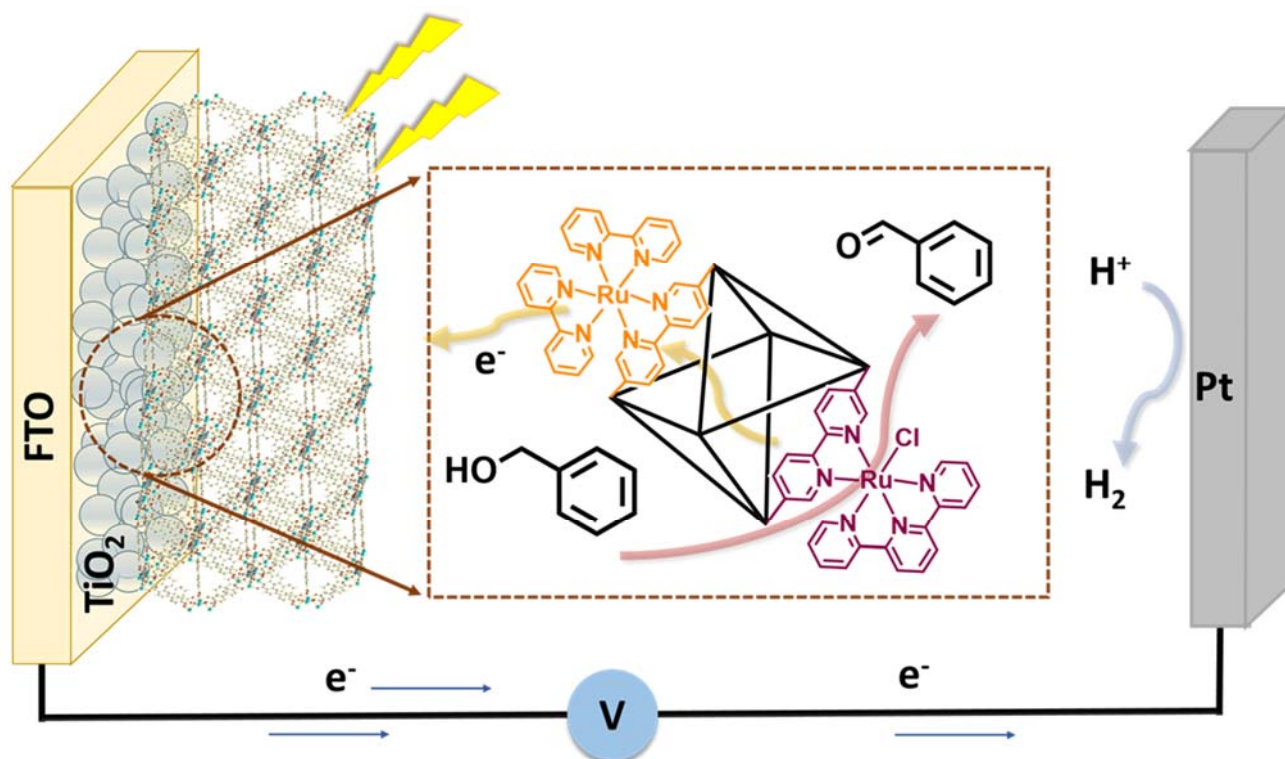
This material is based upon work supported by the Department of Energy under Grant DE-SC0012445.

Notes and references

- 1 H. Furukawa, K. E. Cordova, M. O’Keeffe and O. M. Yaghi, *Science*, 2013, 341, 1230444.
- 2 M. C. So, G. P. Wiederrecht, J. E. Mondloch, J. T. Hupp and O. K. Farha, *Chem. Commun.*, 2015, 51, 3501–3510.
- 3 X. Deng, R. Long, C. Gao and Y. Xiong, *Curr. Opin. Electrochem.*, 2019, 17, 114–120.
- 4 C. Wang, Z. Xie, K. E. deKrafft and W. Lin, *J. Am. Chem. Soc.*, 2011, 133, 13445–13454.
- 5 T. Kajiwara, M. Fujii, M. Tsujimoto, K. Kobayashi, M. Higuchi, K. Tanaka and S. Kitagawa, *Angew. Chemie Int. Ed.*, 2016, 55, 2697–2700.
- 6 C.-C. Hou, T.-T. Li, S. Cao, Y. Chen and W.-F. Fu, *J. Mater. Chem. A*, 2015, 3, 10386–10394.
- 7 D. Kim, D. R. Whang and S. Y. Park, *J. Am. Chem. Soc.*, 2016, 138, 8698–8701.
- 8 S. Yang, D. Fan, W. Hu, B. Pattengale, C. Liu, X. Zhang and J. Huang, *J. Phys. Chem. C*, 2018, 122, 3305–3311.
- 9 S. Yang, B. Pattengale, S. Lee and J. Huang, *ACS Energy Lett.*, 2018, 3, 532–539.
- 10 H. Fei, M. D. Sampson, Y. Lee, C. P. Kubiak and S. M. Cohen, *Inorg. Chem.*, 2015, 54, 6821–6828.
- 11 X. Deng, J. Albero, L. Xu, H. García and Z. Li, *Inorg. Chem.*, 2018, 57, 8276–8286.
- 12 G. Lan, Z. Li, S. S. Veroneau, Y.-Y. Zhu, Z. Xu, C. Wang and W. Lin, *J. Am. Chem. Soc.*, 2018, 140, 12369–12373.
- 13 R. N. Sampaio, D. C. Grills, D. E. Polyansky, D. J. Szalda and E. Fujita, *J. Am. Chem. Soc.*, 2020, 142, 2413–2428.
- 14 J. A. Treadway, J. A. Moss and T. J. Meyer, *Inorg. Chem.*, 1999, 38, 4386–4387.

- 15 M. K. Brennaman, R. J. Dillon, L. Alibabaei, M. K. Gish, C. J. Dares, D. L. Ashford, R. L. House, G. J. Meyer, J. M. Papanikolas and T. J. Meyer, *J. Am. Chem. Soc.*, 2016, 138, 13085–13102.
- 16 F. Mu, B. Dai, W. Zhao, L. Zhang, J. Xu and X. Guo, *Chinese Chem. Lett.*, DOI:https://doi.org/10.1016/j.ccl.2019.12.015.
- 17 A. García-Sánchez, M. Gomez-Mendoza, M. Barawi, I. J. Villar-Garcia, M. Liras, F. Gándara and V. A. de la Peña O'Shea, *J. Am. Chem. Soc.*, 2020, 142, 318–326.
- 18 Y.-J. Dong, J.-F. Liao, Z.-C. Kong, Y.-F. Xu, Z.-J. Chen, H.-Y. Chen, D.-B. Kuang, D. Fenske and C.-Y. Su, *Appl. Catal. B Environ.*, 2018, 237, 9–17.
- 19 J. Zhu, W. A. Maza and A. J. Morris, *J. Photochem. Photobiol. A Chem.*, 2017, 344, 64–77.
- 20 W. A. Maza, R. Padilla and A. J. Morris, *J. Am. Chem. Soc.*, 2015, 137, 8161–8168.
- 21 W. A. Maza and A. J. Morris, *J. Phys. Chem. C*, 2014, 118, 8803–8817.
- 22 W. A. Maza, S. R. Ahrenholtz, C. C. Epley, C. S. Day and A. J. Morris, *J. Phys. Chem. C*, 2014, 118, 14200–14210.
- 23 W. A. Maza, A. J. Haring, S. R. Ahrenholtz, C. C. Epley, S. Y. Lin and A. J. Morris, *Chem. Sci.*, 2016, 7, 719–727.
- 24 S. Lin, A. K. Ravari, J. Zhu, P. M. Usov, M. Cai, S. R. Ahrenholtz, Y. Pushkar and A. J. Morris, *ChemSusChem*, 2018, 11, 464–471.
- 25 S. Lin, Y. Pineda-Galvan, W. A. Maza, C. C. Epley, J. Zhu, M. C. Kessinger, Y. Pushkar and A. J. Morris, *ChemSusChem*, 2017, 10, 514–522.
- 26 S. Lin, P. M. Usov and A. J. Morris, *Chem. Commun.*, 2018, 54, 6965–6974.
- 27 L. Wang, D. L. Ashford, D. W. Thompson, T. J. Meyer and J. M. Papanikolas, *J. Phys. Chem. C*, 2013, 117, 24250–24258.
- 28 D. L. Ashford, W. Song, J. J. Concepcion, C. R. K. Glasson, M. K. Brennaman, M. R. Norris, Z. Fang, J. L. Templeton and T. J. Meyer, *J. Am. Chem. Soc.*, 2012, 134, 19189–19198.
- 29 D. Wang, R. Mendelsohn, E. Galoppini, P. G. Hoertz, R. A. Carlisle and G. J. Meyer, *J. Phys. Chem. B*, 2004, 108, 16642–16653.
- 30 B. V Bergeron and G. J. Meyer, *J. Phys. Chem. B*, 2003, 107, 245–254.
- 31 K. Kalyanasundaram, *Coord. Chem. Rev.*, 1982, 46, 159–244.
- 32 A. J. Morris and G. J. Meyer, *J. Phys. Chem. C*, 2008, 112, 18224–18231.
- 33 A. J. Haring, S. R. Ahrenholtz and A. J. Morris, *ACS Appl. Mater. Interfaces*, 2014, 6, 4394–4401.
- 34 J. Van De Lagemaat and A. J. Frank, 2001, 11194–11205.
- 35 A. Listorti, C. Creager, P. Sommeling, J. Kroon, E. Palomares, A. Fornelli, B. Breen, P. R. F. Barnes, J. R. Durrant, C. Law and B. O'Regan, *Energy Environ. Sci.*, 2011, 4, 3494–3501.

TOC GRAPHIC ENTRY



This work showcases the first instance of cooperative photoelectrochemical oxidation within a chromophore/catalyst-incorporated metal-organic framework.